Progress In Electromagnetics Research, Vol. 167, 111–126, 2020

A Combined Active and Passive Method for the Remote Sensing of Ice Sheet Temperature Profiles

Haokui Xu[1], Leung Tsang[1, *], Joel T. Johnson[2], Kenneth C. Jezek[3], Stephen J. Yan[4], and Prasad Gogineni[4]

Abstract—The Ultra-Wideband Software defined microwave radiometer (UWBRAD) was developed to probe internal ice sheet temperatures using 0.5–2 GHz microwave radiometry. The airborne brightness temperature data of UWBRAD show a significant reduction due to reflections of surface layering of density fluctuations making difficult the retrieval of subsurface temperature in the kilometer range of depth. Such reflections can be measured by the ultra-wideband radar in the same frequency range suggesting a combined active and passive remote sensing of polar ice sheets. In this paper, we develop a coherent reflectivity model for both ice sheet thermal emission and backscattering. Maxwell equations are used to calculate the coherent reflections from the cap layers, and the WKB approximation is used to calculate the transmission for the slowly varying profile below the cap layers. Results are then shown to demonstrate the use of radar measurements to compensate reflection effects on brightness temperatures. It is shown that the reflections corrected brightness temperature is directly related to the physical temperature and absorption profile making possible the retrieval of subsurface temperature profile with multi-frequency measurements.

1. INTRODUCTION

Cryosphere is a critical component of the earth system that continues to experience rapid changes [1, 2]. Mass loss from the Greenland and Antarctic ice sheets is a major contributor to sea level rise [3–7], but ice dynamics and evolution remain incompletely understood and therefore challenging to predict accurately [8, 9]. Recent studies have shown the important impact of ice sheet internal temperatures [10–15], providing new impetus for the development of methods to remotely sense internal ice temperatures. Ice internal temperature contributes to ice stiffness and therefore evolution, but at present remains a quantity that is difficult to measure without in-situ borehole information.

The Ultra-Wideband Software Defined Radiometer (UWBRAD) [16] was developed for sensing internal ice sheet temperature profiles using 0.5–2 GHz microwave radiometry. In principle, the lower UWBRAD frequencies near 0.5 GHz can be impacted by temperatures at depths even greater than 2 kilometers while higher frequencies near 2 GHz respond only to temperatures at shallower depth. UWBRAD has completed airborne campaigns in Greenland in September 2016 and 2017, as well as a deployment to Antarctica in 2018, and has achieved successful measurements of internal ice temperatures under dry snow conditions. However these experiments have shown that firn density fluctuations within the top 100 meters can cause reflections that impact observed brightness temperatures. These effects required UWBRAD temperature profile retrievals to incorporate ancillary information of density

Received 6 March 2020, Accepted 9 August 2020, Scheduled 23 August 2020

* Corresponding author: Leung Tsang (leutsang@umich.edu).

[1] Radiation Laboratory, Department of Electrical Engineering and Computer Science, University of Michigan, Ann Arbor, MI 48109-2122, USA. [2] ElectroScience Laboratory, The Ohio State University, Columbus, OH 43212, USA. [3] School of Earth Science, Byrd Polar Research Center, The Ohio State University, Columbus, OH 43210, USA. [4] Department of Electrical and Computer Engineering, The University of Alabama, Tuscaloosa, AL, USA.

fluctuations. This was accomplished through the use of in-situ borehole measured temperature profiles at location bracketing the flight path, with UWBRAD measurements at these sites used to constrain firn density parameters [17, 18]. Because a-priori information on density fluctuations may not be available for other locations, the development of methods to compensate the impact of firn density variations on brightness temperatures is of interests.

Recent insights into emission physics suggest a means for combining active and passive measurements to reduce or eliminate firn density effects. In this paper, we develop a combined active and passive coherent model for both emission and scattering. The model considers the multiple length scales of density fluctuations in the firn "cap region"; these fluctuations can occur on length scales that are shorter than, comparable to, or greater than the electromagnetic wavelength, so that coherent interactions can be appreciable. We assume that the most impactful density fluctuations occur within the upper 100 m of the ice sheet which is in consistant with the in situ measurements. We also approximate the firn "cap region" as having a uniform temperature, given its limited spatial extent, The "cap region" is further resolved into a large number of layers having different densities as shown in Figure 1. Beneath the cap region, the ice sheet is also assumed inhomogeneous but in this case the permittivity and temperature profiles both vary only on large length scales compared to the electromagnetic wavelength. Rytov's fluctuation dissipation theorem [19, 20] is applicable for computing thermal emission from the lower ice sheet region.

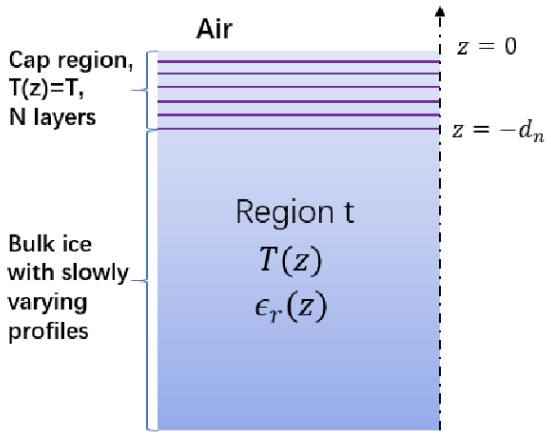

Figure 1. Ice sheet structure.

Due to reciprocity, we solve the active problem first to model radar backscattering at normal incidence by considering plane wave incidence onto the medium of Figure 1, then the passive problem is solved based on the solution of active problem for the thermal emission. Both formulations use a layered medium approach for the cap layers and the WKB approximation for the lower region below the cap layers. Instead of using the explicit form of the dyadic Green's function for a layered medium as in [19, 21], we use only the symmetry properties of the dyadic Green's function. These symmetries allow the solution of passive problem to be expressed entirely in terms of the electromagnetic fields of the active problem. This approach ultimately allows observed brightness temperatures to be expressed in terms of the reflectivity and transmissivity of the cap layers and the microwave emission from the inhomogeneous lower half space. In the retrievals, radar measurements provide information on the reflectivity of the cap layers. Taking advantage of the measurements, the cap layer effects in the measured brightness temperature data are compensated. The compensated data, as shown in the model, is directly related to the ice sheet physical temperature and absorption profiles.

The organization of the paper is as follows. In Section 2, we consider problem A, representing active remote sensing using a wave radiated from a source above the ice sheet that is far from the observation area. The result is a plane wave incident upon the observation area, and the electric field inside the inhomogeneous layered medium is expressed in terms of the dyadic Green's function with a source in the free space region and an observation point within the ice sheet layered medium. In Section 3, we consider problem B representing passive microwave remote sensing, with microwave thermal emission expressed

in terms of sources obtained from Rytov's fluctuation dissipation theorem. Brightness temperatures are then expressed in terms of the dyadic Green's function for sources within the layered medium. Using the symmetry properties of the dyadic Green's function (see Appendix), the brightness temperatures of problem B are then expressed in terms of the electric fields of Problem A. In Section 5, we then derive the solution of Problem A using Maxwell equations and the WKB approximation for the lower half space under vertically polarized incidence (TM) and then shows that the brightness temperature can then be expressed in terms of the reflectivity and transmissivity from problem A and the microwave thermal emission from the lower half space. Numerical results for both cases are provided in Section 6 followed by concluding remarks.

2. ACTIVE PROBLEM A

Consider a short electric dipole antenna having dipole moment $\widehat{\alpha} Id\ell$ located at position $\overline{r}_0$ with $\widehat{r}_0$ a unit vector from the origin to the dipole location (Figure 2). The distance r_0 is far away from the observation area. The resulting incident electric field at position $\overline{r}$ in Region 0 is:

$$\overline{E}_{inc}^{(A)} = i\omega\mu Id\ell\overline{\overline{G}}_0\left(\overline{r}, \overline{r}_0\right) \cdot \widehat{\alpha} \tag{1}$$

where $\overline{\overline{G}}_0$ is the free space dyadic Green's function which can be approximated locally about the origin as a plane wave having polarization $\widehat{\alpha}$:

$$\overline{E}_{inc}^{(A)} = i\omega\mu\frac{\exp\left(ikr_0\right)}{4\pi r_0} Id\ell\widehat{\alpha}\exp\left(i\overline{k}_i \cdot \overline{r}\right) \tag{2}$$

where $\widehat{k}_i = -\widehat{r}_0$ and $\overline{k}_i = k\widehat{k}_i$, we choose $Id\ell$ such that

$$i\omega\mu\frac{\exp\left(ikr_0\right)}{4\pi r_0} Id\ell = 1 \tag{3}$$

so that the incident wave is of unit amplitude:

$$\overline{E}_{inc}^{(A)} = \widehat{\alpha}\exp\left(i\overline{k}_i \cdot \overline{r}\right) \tag{4}$$

Now $\overline{E}_1^{(A)}$, the electric field in region 1 that results, can be expressed in terms of the layered medium dyadic Green's function $\overline{\overline{G}}_{10}$:

$$\overline{E}_1^{(A)}\left(\overline{r}\right) = i\omega\mu Id\ell\overline{\overline{G}}_{10}\left(\overline{r}, \overline{r}_0\right) \cdot \widehat{\alpha} \tag{5}$$

where the subscript 10 denotes an observation point in region 1 and a source in region 0. Using the amplitude of $Id\ell$ we have

$$\left|\overline{E}_1^{(A)}\left(\overline{r}\right)\right|^2 = \left(4\pi r_0\right)^2\left|\overline{\overline{G}}_{10}\left(\overline{r}, \overline{r}_0\right) \cdot \widehat{\alpha}\right|^2 \tag{6}$$

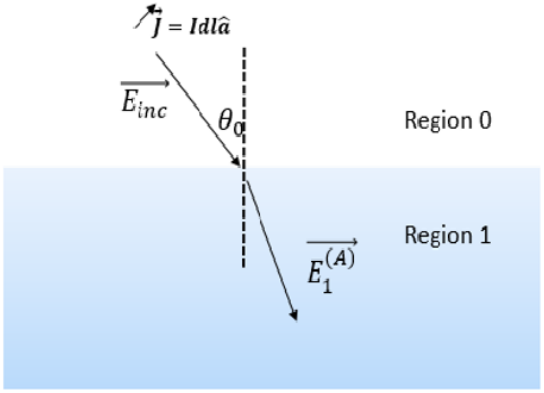

Figure 2. Problem A.

Similar Green's functions also exist to determine the resulting fields in any other layer within the modeled ice sheet.

3. PASSIVE PROBLEM B

The passive problem is shown in Figure 3. The antenna in θ_0 direction receives the thermal emission from region 0 with brightness temperature T_B. For passive remote sensing, thermal emission can be modeled as arising from noise current sources in the layered medium whose covariance is related to the medium physical temperature $T(\overline{r}\,')$ using Rytov's fluctuation dissipation theorem [22]

$$\left\langle \overline{J}_{1B}\left(\overline{r}\,',\omega\right)\overline{J}_{1B}^{*}\left(\overline{r}\,'',\omega'\right)\right\rangle = \frac{4}{\pi}\omega\varepsilon_1''\left(\overline{r}\,'\right)K_BT\left(\overline{r}\,'\right)\overline{\overline{I}}\delta\left(\omega-\omega'\right)\delta\left(\overline{r}\,'-\overline{r}\,''\right) \tag{7}$$

Here K_B represents Boltzmann's constant; ω represents the angular frequency; ϵ'' represents the imaginary part of the medium permittivity; $\overline{\overline{I}}$ is the unit tensor so that vector current components are uncorrelated. The quantity of interest in problem B is the covariance of the electric field emitted into region 0 and its integration over the observed bandwidth:

$$\int_{\Delta\omega} d\omega \left\langle \overline{E}_0^{(B)}\left(\overline{r}_0,\omega\right)\cdot\overline{E}_0^{(B)*}\left(\overline{r}_0,\omega'\right)\right\rangle_{th} \tag{8}$$

Note that we put the "radiometer receiver" at the same place as the transmitter antenna of problem (A). Then the electric field in region 0 in $\widehat{\alpha}$ polarization is:

$$\widehat{\alpha}\cdot\overline{E}_0^{(B)}\left(\overline{r}_0,\omega\right) = i\omega\mu\int d\overline{r}\,'\left(\widehat{\alpha}\cdot\overline{\overline{G}}_{01}\left(\overline{r}_0,\overline{r}\,',\omega\right)\right)\cdot\overline{J}_{1B}\left(\overline{r}\,',\omega\right) \tag{9}$$

where $\overline{\overline{G}}_{01}$ is the dyadic Green's function with the source in region 1 and observation point in region 0. Using this expression and taking the ensemble average yields [19]:

$$\begin{aligned}&\left\langle\left(\widehat{\alpha}\cdot\overline{E}_0^{(B)}\left(\overline{r},\omega\right)\right)\left(\widehat{\alpha}\cdot\overline{E}_0^{(B)*}\left(\overline{r},\omega'\right)\right)\right\rangle\\ &= \omega\mu\omega'\mu\int d\overline{r}\,''\int d\overline{r}\,'\left(\widehat{\alpha}\cdot\overline{\overline{G}}_{01}\left(\overline{r}_0,\overline{r}\,',\omega\right)\right)\cdot\left\langle\overline{J}_{1B}\left(\overline{r}\,',\omega\right)\overline{J}_{1B}\left(\overline{r}\,'',\omega'\right)\right\rangle\cdot\left(\widehat{\alpha}\cdot\overline{\overline{G}}_{01}^{*}\left(\overline{r}_0,\overline{r}\,'',\omega'\right)\right)\end{aligned} \tag{10}$$

note that the correlation of noise currents gives a $\delta(\omega-\omega')$, and we integrate over a small bandwidth for the value field correlation at frequency ω:

$$\begin{aligned}&\int_{\Delta\omega} d\omega\left\langle\left(\widehat{\alpha}\cdot\overline{E}_0^{(B)}\left(\overline{r}_0,\omega\right)\right)\left(\widehat{\alpha}\cdot\overline{E}_0^{(B)*}\left(\overline{r}_0,\omega'\right)\right)\right\rangle\\ &= \omega^2\mu^2\int d\overline{r}\,'\left|\widehat{\alpha}\cdot\overline{\overline{G}}_{01}\left(\overline{r}_0,\overline{r}\,',\omega\right)\right|^2\frac{4}{\pi}\omega\varepsilon_1''\left(\overline{r}\,'\right)K_BT\left(\overline{r}\,'\right)\end{aligned} \tag{11}$$

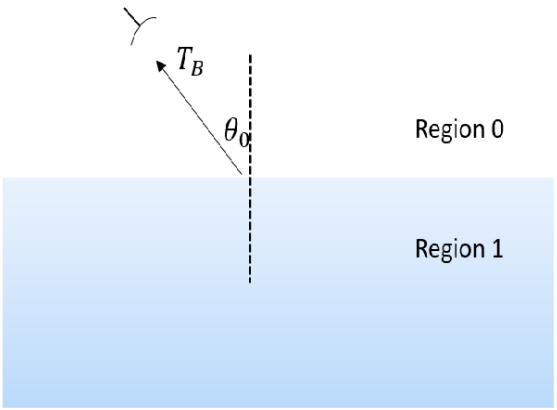

Figure 3. Problem B.

Appendix A shows that,

$$\overline{\overline{G}}_{01}\left(\overline{r}_a,\overline{r}_b\right)=\overline{\overline{G}}_{10}^{t}\left(\overline{r}_b,\overline{r}_a\right) \tag{12}$$

so that

$$\begin{aligned}&\int_{\Delta\omega}d\omega\left\langle\left(\widehat{\alpha}\cdot\overline{E}_0^{(B)}\left(\overline{r},\omega\right)\right)\left(\widehat{\alpha}\cdot\overline{E}_0^{(B)*}\left(\overline{r},\omega'\right)\right)\right\rangle\\ &=\omega^2\mu^2\int d\overline{r}\,'\left|\left(\overline{\overline{G}}_{10}\left(\overline{r}\,',\overline{r}_0,\omega\right)\cdot\widehat{\alpha}\right)\right|^2\frac{4}{\pi}\omega\varepsilon_1''\left(\overline{r}\,'\right)K_BT\left(\overline{r}\,'\right)\end{aligned} \tag{13}$$

From problem A, we have

$$\left|\overline{E}_1^{(A)}\left(\overline{r}\right)\right|^2=\left(4\pi r_0\right)^2\left|\overline{\overline{G}}_{10}\left(\overline{r},\overline{r}_0\right)\cdot\widehat{\alpha}\right|^2 \tag{14}$$

so that

$$\begin{aligned}&\int_{\Delta\omega}d\omega\left\langle\left(\widehat{\alpha}\cdot\overline{E}_0^{(B)}\left(\overline{r},\omega\right)\right)\left(\widehat{\alpha}\cdot\overline{E}_0^{(B)*}\left(\overline{r},\omega'\right)\right)\right\rangle\\ &=\omega^2\mu^2\frac{1}{\left(4\pi r_0\right)^2}\int d\overline{r}\,'\left|\overline{E}_1^{(A)}\left(\overline{r}\,'\right)\right|^2\frac{4}{\pi}\,\omega\varepsilon_1''\left(\overline{r}\,'\right)K_BT_B\left(\overline{r}\,'\right)\end{aligned} \tag{15}$$

The power received in polarization α is also

$$P_\alpha=\lim_{r_0\to\infty}r_0^2d\Omega\int_{\Delta\omega}d\omega\int_{\Delta\omega}d\omega'\frac{\left\langle\left(\widehat{\alpha}\cdot\overline{E}_0^{(B)}\left(\overline{r}_0,\omega\right)\right)\left(\widehat{\alpha}\cdot\overline{E}_0^{(B)*}\left(\overline{r}_0,\omega'\right)\right)\right\rangle}{2\eta}$$

which can be rewritten as [19]:

$$P_\alpha=\Delta\omega d\Omega\mu\frac{1}{\lambda^2}\frac{1}{\pi}\,\omega\frac{1}{2\eta}\int d\overline{r}\,'\left|\overline{E}_1^{(A)}\left(\overline{r}\,'\right)\right|^2\frac{\varepsilon_1''\left(\overline{r}\,'\right)}{\varepsilon_0}K_BT\left(\overline{r}\,'\right)$$

This received power can be re-scaled into the observed brightness temperature through:

$$P_\alpha=\frac{K_BT_{B\alpha}}{\lambda^2}\,d\Omega\frac{\Delta\omega}{2\pi}A_0\cos\theta_0 \tag{16}$$

where θ_0 is the observation angle, and $T_{B\alpha}$ is the brightness temperature in α polarization.

The final brightness temperature in direction $\widehat{r}_0=-\widehat{k}_i$ is then

$$T_{B\alpha}\left(\widehat{r}_0\right)=\frac{1}{A_0\cos\theta_0}k\int d\overline{r}\,'\left|\overline{E}_1^{(A)}\left(\overline{r}\,'\right)\right|^2\frac{\epsilon_1''\left(\overline{r}\,'\right)}{\varepsilon_0}T\left(\overline{r}\,'\right) \tag{17}$$

The above expression gives the brightness temperature of problem B in terms of the electric field in region 1 of problem A. Note that this eliminates the use of an explicit form of the dyadic Green's functions as used in previous papers [20, 22]. A similar approach can be used to relate the fields within other layers of the layered medium to their brightness temperature contributions.

4. EMISSION FROM LAYERED MEDIUM OVER AN INHOMOGENEOUS HALF SPACE

As shown in Figure 1, we model the firn cap layer as N regions with reflective boundaries, with Region 0 corresponding to the free space region. The regions are labelled as $\ell=1,2,...,N$, with the number of layers N on the order of hundreds with each region thickness on the order of centimeters or finer.

The layer boundaries are located at $z=0,-d_1,.....,-d_N$, and for each region ℓ, the permittivity is written as ε_ℓ. Within the cap region, the temperature T is modeled as uniform. For the region $t=N+1$, below $z=-d_N$, the permittivity $\varepsilon_t(z)$ is a slowly varying function of z and the temperature profile $T(z)$ is a slowly varying function of z. In this region, we use the WKB method for analyzing the

internal fields under the assumption that there are no further reflections. and that the last boundary $z = -d_N$ is reflectionless. Now we define:

$$\begin{aligned} T_{B\alpha}(\widehat{r}_0) &= T^u_{B\alpha}(\widehat{r}_0) + T^l_{B\alpha}(\widehat{r}_0) \\ T^u_{B\alpha}(\widehat{r}_0) &= \textit{contribution from the cap N layers} \\ T^l_{B\alpha}(\widehat{s}_0) &= \textit{contribution from region t, the inhomogeneous lower half space} \end{aligned}$$

$$T^l_{B\alpha}(\widehat{s}_0) = \frac{k}{A_0 \cos\theta_0} \int_{z\le -d_N} d\overline{r} \varepsilon''_{1r}(\overline{r}) T(\overline{r}) \left| \overline{E}^{(A)}_1(\overline{r}\,') \right|^2 \tag{18}$$

$$T^u_{B\alpha}(\widehat{s}_0) = \frac{k}{A_0 \cos\theta_0} T \int_{z\ge -d_N}^{0} d\overline{r} \epsilon''_{1r}(\overline{r}) \left| \overline{E}^{(A)}_1(\overline{r}\,') \right|^2 \tag{19}$$

The time-averaged Poynting vector in problem A is $\overline{S}^{(A)} = \frac{1}{2}\left\{\overline{E}^{(A)} \times \overline{H}^{(A)*}\right\}$ for fields in region 0, and can be similarly defined as $\overline{S}^{(A)}_1$ in region 1. Then by the Poynting theorem

$$\nabla \cdot \left(\overline{S}^{(A)}_1\right) = -\frac{1}{2}\omega\epsilon\epsilon''_{1r}(\overline{r}) \overline{E}^{(A)}_1 \cdot \overline{E}^{(A)*}_1 \tag{20}$$

Substituting for the field amplitude squared in Eq. (20) and applying the divergence theorem then yields

$$T^u_{B\alpha}(\widehat{s}_0) = \frac{1}{A_0 \cos\theta_0} T 2\eta \left[\int_{S_u} dS \left(-\widehat{n} \cdot \left(\overline{S}^{(A)}\right)\right) + \int_{S_l} dS \widehat{n} \cdot \left(\overline{S}^{(A)}_1\right)\right] \tag{21}$$

where $\widehat{n}$ is pointing up on both the upper and lower boundaries, S_u at $z = 0$ and S_1 at $z = -d_N$. In the above, we have also made use of the relation: $\widehat{n} \cdot \overline{S}^{(A)}_1 = \widehat{n} \cdot \overline{S}^{(A)}$ because of continuity of tangential electric fields and magnetic fields at the boundary.

5. TM CASE: VERTICAL POLARIZATION

In this section we consider vertically polarized (TM) plane wave incidence in Problem A. For a field incident in the (x-z) plane, the incident k-vector can be written as

$$\overline{k}_i = \widehat{x} k_x - \widehat{z} k_z = \widehat{x} k \sin\theta_0 - \widehat{z} k \cos\theta_0$$

For a unit amplitude incident electric field, the incident magnetic field has amplitude $1/\eta$ where $\eta = \sqrt{\mu/\varepsilon}$ and has only $\widehat{y}$ component:

$$\overline{H}^{(A)}_i = \widehat{y} \exp \frac{1}{\eta} (ik_x x - ik_z z) \tag{22}$$

The reflected wave in region 0 is then

$$\overline{H}^{(A)}_r = \widehat{y} R^{TM}_{cap} \exp(ik_x x + ik_z z) \tag{23}$$

and the Poynting vector $\overline{S}^{(A)}$ in medium 0 is

$$-\widehat{z} \cdot \left(\overline{S}^{(A)}\right) = \frac{\cos\theta_0}{2\eta} \left[1 - \left|R^{TM}_{cap}\right|^2\right] \tag{24}$$

Using $\int_{S_u} dS = A_0$, we have

$$T^u_{B\alpha}(\widehat{r}_0) = T\left[1 - \left|R^{TM}_{cap}\right|^2\right] + \frac{T}{A_0 \cos\theta_0} 2\eta \int_{S_l} dS \widehat{n} \cdot \left(\overline{S}^{(A)}_1\right) \tag{25}$$

$$T^l_{B\alpha}(\widehat{r}_0) = \frac{k}{A_0 \cos\theta_0} \int_{z\le -d_N} d\overline{r} \varepsilon''_{1r}(\overline{r}) T(\overline{r}) \left| \overline{E}^{(A)}_1(\overline{r}) \right|^2 \tag{26}$$

where Equation (25) is the thermal emission from cap region from Equation (21), and Equation (26) is the thermal emission from the bulk ice region by applying Equation (18).

5.1. Fields within the Cap Region

For region ℓ, $H_{\ell y}$ and $E_{\ell x}$ have the form:

$$\begin{aligned} H_{\ell y} &= \frac{1}{\eta}\left[C_\ell \exp\left(ik_{\ell z}z\right) + D_\ell \exp\left(-ik_{\ell z}z\right)\right]\exp\left(ik_x x\right) \\ E_{\ell x} &= \frac{\varepsilon}{k}\frac{k_{\ell z}}{\varepsilon_\ell}\left[C_\ell \exp\left(ik_{\ell z}z\right) - D_\ell \exp\left(-ik_{\ell z}z\right)\right]\exp\left(ik_x x\right) \end{aligned}$$

The coefficients C_ℓ and D_ℓ can be determined by matching the boundary conditions at each interface:

$$\left[C_\ell \exp\left(-ik_{\ell z}d_\ell\right) + D_\ell \exp\left(ik_{\ell z}d_\ell\right)\right] = \left[C_{\ell+1}\exp\left(-ik_{(\ell+1)z}d_\ell\right) + D_{\ell+1}\exp\left(ik_{(\ell+1)z}d_\ell\right)\right] \quad (27)$$

$$\frac{k_{lz}}{\epsilon_l}\left[C_\ell \exp\left(-ik_{\ell z}d_\ell\right) - D_\ell \exp\left(ik_{\ell z}d_\ell\right)\right] = \frac{k_{(l+1)z}}{\epsilon_(l+1)}\left[C_{\ell+1}\exp\left(-ik_{\ell+1z}d_\ell\right) - D_{\ell+1}\exp\left(ik_{\ell+1z}d_{\ell+1}\right)\right] \quad (28)$$

with $d_0 = 0$

$$\begin{aligned} D_0 &= 1 \\ C_0 &= R_{cap}^{TM} \end{aligned}$$

Here R_{cap}^{TM} is the reflection coefficient of the cap region, which includes multiple boundaries. The boundary $z = -d_N$ separates regions N and $t = N+1$. At the interface of the cap and lower regions, we let

$$\begin{aligned} \varepsilon_{t0} &= \varepsilon_t\left(z = -d_N\right) \\ k_{tz0} &= \sqrt{k^2\varepsilon_{t0} - k_x^2} \end{aligned}$$

so that near $z = -d_N$

$$H_{ty} = \frac{1}{\eta}\left[T_{cap}^{TM}\exp\left(-ik_{tz0}z\right)\right]\exp\left(ik_x x\right) \quad (29)$$

$$E_{tx} = \frac{\varepsilon}{k}\frac{k_{tz}}{\varepsilon_{t0}}\left[-T_{cap}^{TM}\exp\left(-ik_{\ell z}z\right)\right]\exp\left(ik_x x\right) \quad (30)$$

where

$$\begin{aligned} D_t &= T_{cap}^{TM} \\ C_t &= 0 \end{aligned}$$

Here T_{cap}^{TM} is the transmission coefficient of the cap region. Matching at $z = -d_N$ then yields

$$\left[C_N \exp\left(-ik_{Nz}d_N\right) + D_N \exp\left(ik_{Nz}d_N\right)\right] = \left[T_{cap}^{TM}\exp\left(ik_{tz0}d_N\right)\right] \quad (31)$$

$$\frac{k_{Nz}}{\varepsilon_N}\left[C_N \exp\left(-ik_{Nz}d_N\right) - D_N \exp\left(ik_{Nz}d_N\right)\right] = \frac{k_{tz0}}{\varepsilon_{t0}}\left[-T_{cap}^{TM}\exp\left(ik_{tz0}d_N\right)\right] \quad (32)$$

The reflection coefficient in each layer can now be calculated by recurrence using

$$R_{\ell(\ell+1)}^{TM} = \frac{\varepsilon_{(\ell+1)}k_{\ell z} - \varepsilon_\ell k_{(\ell+1)z}}{\varepsilon_{(\ell+1)}k_{\ell z} + \varepsilon_\ell k_{(\ell+1)z}}$$

where $\ell = 0, 1, ..., N-1$ with $R_{Nt}^{TM} = \frac{\varepsilon_{t0}k_{Nz} - \varepsilon_N k_{tz0}}{\varepsilon_{t0}k_{Nz} + \varepsilon_N k_{tz0}}$.

Finally defining $q_\ell = \frac{C_\ell}{D_\ell}\exp(-2ik_{\ell z}d_\ell)$ the recurrence relation is

$$q_\ell = \frac{q_{\ell+1}\exp\left(2ik_{(\ell+1)z}\left(d_{\ell+1} - d_\ell\right)\right) + R_{\ell(\ell+1)}^{TM}}{R_{\ell(\ell+1)}^{TM}q_{\ell+1}\exp\left(2ik_{(\ell+1)z}\left(d_{\ell+1} - d_\ell\right)\right) + 1} \quad (33)$$

Starting with $q_N = R_{Nt}^{TM}$ we move up until we get $q_0 = R_{cap}^{TM}$. We then propagate down to determine T_{cap}^{TM} for $\ell = 0, 1, 2, ..., N$

$$C_{\ell+1}\exp\left(-ik_{(\ell+1)z}d_\ell\right) = \frac{1}{2}C_\ell\exp\left(-ik_{\ell z}d_\ell\right)\left[1+\frac{\varepsilon_{\ell+1}k_{\ell z}}{k_{(\ell+1)z}\varepsilon_\ell}\right]+\frac{1}{2}D_\ell\exp\left(ik_{\ell z}d_\ell\right)\left[1-\frac{\varepsilon_{\ell+1}k_{\ell z}}{k_{(\ell+1)z}\varepsilon_\ell}\right]$$
$$D_{\ell+1}\exp\left(ik_{(\ell+1)z}d_\ell\right) = \frac{1}{2}C_\ell\exp\left(-ik_{\ell z}d_\ell\right)\left[1-\frac{\varepsilon_{\ell+1}k_{\ell z}}{k_{(\ell+1)z}\varepsilon_\ell}\right]+\frac{1}{2}D_\ell\exp\left(ik_{\ell z}d_\ell\right)\left[1+\frac{\varepsilon_{\ell+1}k_{\ell z}}{k_{(\ell+1)z}\varepsilon_\ell}\right]$$

until we get to

$$D_t = T_{cap}^{TM}$$
$$C_t = 0$$

Just below $z = -d_N$, the Poynting vector $\overline{S}_1^{(A)}$ is

$$\widehat{z}\cdot\overline{S}_1^{(A)} = -\frac{1}{2}\frac{\varepsilon}{k}\mathrm{Re}\left(\frac{1}{\eta}\frac{k_{tz0}}{\varepsilon_{t0}}\left|T_{cap}^{TM}\right|^2\exp\left(-2k''_{tz0}d_N\right)\right)$$

After solving the Poynting's vector at $z = -d_N$, we apply Equation (25) for the thermal emission of cap region.

$$T_{B\alpha}^u\left(\widehat{s}_0\right) = T\left[1-\left|R_{cap}^{TM}\right|^2\right]-T\frac{1}{k\cos\theta_0}\mathrm{Re}\left(\frac{\varepsilon k_{tz0}}{\varepsilon_{t0}}\left|T_{cap}^{TM}\right|^2\exp\left(-2k''_{tz0}d_N\right)\right) \tag{34}$$

Let

$$t_{cap}^{TM} = \frac{1}{k\cos\theta_0}\mathrm{Re}\left(\frac{\varepsilon k_{tz0}}{\varepsilon_{t0}}\left|T_{cap}^{TM}\right|^2\exp\left(-2k''_{tz0}d_N\right)\right)$$
$$r_{cap}^{TM} = \left|R_{cap}^{TM}\right|^2$$

Then the contribution from cap region is given by:

$$T_{B\alpha}^u\left(\widehat{s}_0\right) = T\left[1-r_{cap}^{TM}-t_{cap}^{TM}\right] \tag{35}$$

5.2. WKB for Region *t*

Region t has the permittivity profile $\varepsilon_t(z)$. For the TM case, the $\widehat{y}$ component of the magnetic field in region t obeys the equation:

$$\varepsilon_t(z)\frac{\partial}{\partial z}\frac{1}{\varepsilon_t(z)}\frac{\partial H_{ty}}{\partial z}-k_x^2H_{ty} = -k^2\frac{\varepsilon_t(z)}{\varepsilon}H_{ty} \tag{36}$$

with k_x fixed according to phase matching. Defining $k_t(z) = k\sqrt{\frac{\varepsilon_t(z)}{\varepsilon}}$ we have a differential equation for H_{ty}.

$$\frac{\partial^2H_{ty}}{\partial z^2}-\frac{1}{\epsilon_t(z)}\left(\frac{\partial\epsilon_t(z)}{\partial z}\right)\left(\frac{\partial H_{ty}}{\partial z}\right)+\frac{1}{\delta^2}k_{tz}^2(z)H_{ty} = 0 \tag{37}$$

In the above equation, we have inserted the ordering "δ" parameter which is a small number. In the WKB method, we assume that H_{ty} is of the form:

$$H_{ty} = \exp\left(\frac{1}{\delta}\sum_{n=0}^{\infty}\delta^nS_n(z)\right) \tag{38}$$

Substituting in, we obtain

$$\left(\frac{1}{\delta}\sum_{m=0}^{\infty}\delta^mS_m''(z)\right)+\left(\frac{1}{\delta}\sum_{m=0}^{\infty}\delta^mS_m'(z)\right)^2+\frac{1}{\delta^2}k_{tz}^2(z)-\frac{1}{\varepsilon_t(z)}\left(\frac{\partial\varepsilon_t(z)}{\partial z}\right)\left(\frac{1}{\delta}\sum_{m=0}^{\infty}\delta^mS_m'(z)\right) = 0 \tag{39}$$

First, we balance the equation to the order of $\frac{1}{\delta^2}$

$$\left(S_0'(z)\right)^2 + k_{tz}^2(z) = 0 \tag{40}$$

and determine the solution at this order for a wave propagating downward

$$S_0(z) = i\int_z^{-d_N} dz' k_{tz}(z') \tag{41}$$

Next we balance to order $\frac{1}{\delta}$:

$$2S_0'(z)S_1'(z) = -S_0''(z) + \frac{1}{\varepsilon_t(z)}\left(\frac{\partial \varepsilon_t(z)}{\partial z}\right)\left(S_0'(z)\right) \tag{42}$$

and match the coefficient to the magnetic field at $z = -d_N$. Then

$$H_{ty}(z) = \frac{T^{TM}\exp\left(ik_{tz0}d_N\right)}{\eta\left(\left(\frac{\varepsilon_{t0}^2}{-k_{tz0}^2}\right)\right)^{1/4}} \frac{1}{\left(\left(\frac{-k_{tz}^2(z)}{\varepsilon_t^2(z)}\right)\right)^{1/4}} \exp\left(i\int_z^{-d_N} dz' k_{tz}(z')\right) \tag{43}$$

To calculate $T_{B\alpha}^l(\widehat{r}_0) = \frac{k}{\cos\theta_0}\int_{-\infty}^{-d_N} dz\epsilon_{1r}''(z)T(z)|\overline{E}_1^{(A)}(\overline{r})|^2$ we use $|\overline{E}_1^{(A)}(\overline{r})|^2 = |E_{tx}|^2 + |E_{tz}|^2$. The thermal emission from the inhomogeneous half space is then given by:

$$\begin{aligned} T_{B\alpha}^l(\widehat{r}_0) \;=\; & \frac{k}{\cos\theta_0}\int_{-\infty}^{-d_N} dz\varepsilon_{1r}''(z)\,T(z) \\ & \left|\frac{T_{cap}^{TM}}{\eta\left(\left(\frac{\varepsilon_{t0}^2}{-k_{tz0}^2}\right)\right)^{1/4}}\right|^2 \left[\left|\frac{k_{tz}(z)}{\omega\varepsilon_t(z)}\right|^2 + \left|\frac{k_x}{\omega\varepsilon_t(z)}\right|^2\right] \frac{\exp\left(-2k_{tz0}''d_N - \int_z^{-d_N} dz' 2k_{tz}''(z')\right)}{\left|\left(\left(\frac{-k_{tz}^2(z)}{\varepsilon_t^2(z)}\right)\right)^{1/4}\right|^2} \end{aligned}$$

Note that

$$t_{cap}^{TM} = \frac{1}{k\cos\theta}\mathrm{Re}\left(\frac{\epsilon k_{tz0}}{\epsilon_{t0}}|T_{cap}^{TM}|^2\exp(-2k_{tz0}''d_N)\right)$$

The equation becomes:

$$\begin{aligned} T_{B\alpha}^l(\widehat{r}_0) \;=\; & k^2 t_{cap}^{TM}\int_{-\infty}^{-d_N} dz\varepsilon_{1r}''(z)\,T(z) \\ & \frac{\epsilon(t)}{\eta^2\epsilon}\left[\left|\frac{k_{tz}(z)}{\omega\varepsilon_t(z)}\right|^2 + \left|\frac{k_x}{\omega\varepsilon_t(z)}\right|^2\right]\exp\left(-2k_{tz0}''d_N - \int_z^{-d_N} dz' 2k_{tz}''(z')\right) \end{aligned}$$

Using the fact that $|k_{tz}(z)|^2 + k_x^2 = k_t^2$ and $\omega^2\mu\epsilon_t(z) = k_t^2(z)$. The equation is further simplified into:

$$\begin{aligned} T_{B\alpha}^l(\widehat{r}_0) \;=\; & \frac{k^2 t_{cap}^{TM}}{k_{t0}cos\theta_{t0}}\int_{-\infty}^{-d_N} dz\varepsilon_{1r}''(z)\,T(z) \\ & \frac{k_{tz0}}{k_{tz}(z)}\exp\left(-2k_{tz0}''d_N - \int_z^{-d_N} dz' 2k_{tz}''(z')\right) \end{aligned}$$

where k_tz0 is the value of k_tz at $z = -d_N$. Note that $2k_t'(1)k_t''(z) = k^2\epsilon_{1r}''$ and $2k_{tz}'(1)k_{tz}''(z) = k^2\epsilon_{1r}''$ and use the relationship $k_{tz}'(z) = k_t' = k_t'(z)\cos\theta_t(z)$. The equation is simplified into:

$$T_{B\alpha}^l(\widehat{r}_0) = t^{TM}\int_{-\infty}^{-d_N} dz T(z)\,2k_t''(z)\sec\theta_t(z)\exp\left(-\int_z^{-d_N} dz' k_{tz}''(z')\right) \tag{44}$$

Finally, we have $k_{(}''tz) = k_t'' \sec\theta_t(z)$ and $k_t'' = \frac{\kappa_a(z)}{2}$. Then brightness temperature given by the lower half space is:

$$T_{B\alpha}^l(\widehat{r}_0) = t^{TM} \int_{-\infty}^{-d_N} dz T(z) \kappa_a(z) \sec\theta_t(z) \exp\left(-\int_z^{-d_N} dz' \kappa_a(z') \sec\theta_t(z')\right) \quad (45)$$

Summing the contributions from the cap layers and the lower half space we have:

$$T_{B\alpha}(\widehat{s}_0) = T\left[1 - r^{TM} - t^{TM}\right] + t^{TM} \int_{-\infty}^{-d_N} dz \kappa_a(z) \sec\theta_t(z) T_t(z) \exp\left(-\int_z^{-d_N} dz' \kappa_a(z') \sec\theta_t(z')\right) \quad (46)$$

The above gives the expression of the coherent model in terms of Eq. (1) the reflectivity and transmissivity of the cap layers and Eq. (2) the absorption and temperature profile of the lower half space. In general r^{TM} and t^{TM} are complicated and are dependent on the density fluctuations. However, if they are measured by a radar, then the above formula can be used to retrieve the temperature profile in the second term from the brightness temperature measurements.

If it is assumed that the absorption in cap layers is weak, we can further approximate: $1 - r^{TM} - t^{TM} = 0$ to obtain

$$T_{B\alpha}(\widehat{s}_0) = (1 - r^{TM}) \int_{-\infty}^{-d_N} dz \kappa_a(z) \sec\theta_t(z) T_t(z) \exp\left(-\int_z^{-d_N} dz' \kappa_a(z') \sec\theta_t(z')\right) \quad (47)$$

Obviously, the brightness temperature from the ice body is reduced by the cap layer reflections. If we compensate these reflection effects, the brightness temperature is related only to the ice sheet physical temperature and absorption profiles.

The solution for horizontal polarization (TE) can be obtained similarly and yields a solution identical to that of Eqs. (46)–(47) if the TE polarized reflection and transmission coefficients are used.

6. NUMERICAL SIMULATIONS

Numerical results for ice sheet thermal emission are presented in this section. The density profile $\rho(z)$ of the ice sheet is simulated using the density model of [20, 22], in which:

$$\begin{aligned} \rho(z) &= \overline{\rho}(z) + \rho_n(z) \\ \rho_n(z) &= \rho_n^{(1)}(z) \exp(\frac{z}{\alpha_1}) \\ \left\langle \rho_n^{(1)}(z) \rho_n^{(1)}(z') \right\rangle &= \Delta_1^{(1)} \exp\left(-\frac{(z-z')^2}{\ell_1^2}\right) \end{aligned}$$

where $\overline{\rho}(z)$ is the mean density profile described by $\overline{\rho}(z) = 0.922 - 0.564\exp(0.0165z)$ while the fluctuating part $\rho_n(z)$ is a stationary Gaussian random process characterized by 3 parameters Δ_1, the variance, ℓ_1, the correlation length, and α_1 the damping factor for the fluctuations. Figure 4 illustrates an example of simulated density profile. The fluctuations in density over a range of length scales is evident. The physical temperature profile of the ice sheet is described by the Robin temperature model [23]:

$$T(z) = T_s + C \cdot \mathrm{erf}\left(\frac{H}{L}\right) - C \cdot \mathrm{erf}\left(\frac{z+H}{L}\right), \quad -H \le z \le 0 \quad (48)$$

where $C = \frac{LG\sqrt{\pi}}{2k_c}$, and erf is the error function. Here $k_c = 2.7\,\mathrm{W/m}$ is the ice thermal conductivity $k_d = 45\,\mathrm{sqm/year}$ is the ice thermal diffusivity, and T_s is the surface temperature of the ice sheet. Also, M is the mass accumulation rate, G the geothermal heat flux, and H the total thickness of the ice sheet. We choose $T_s = 216\,\mathrm{K}$, $M = 0.01\,\mathrm{m/year}$, $G = 0.047\,\mathrm{W/sqm}$ and $H = 3700\,\mathrm{m}$ in what follows. The simulated temperature profile with the given parameters are shown in Figure 5. The parameters for generating density profiles are the same as in Figure 4. The permittivity of the ice sheet is calculated using the Matzler [24, 25] and Tiuri [26] formulas for the real part and imaginary part, respectively.

Figure 6 plots the simulated brightness temperature from 0.5 to 2 GHz for both the standard coherent model and the coherent reflectivity model derived in this paper following an average over 1000

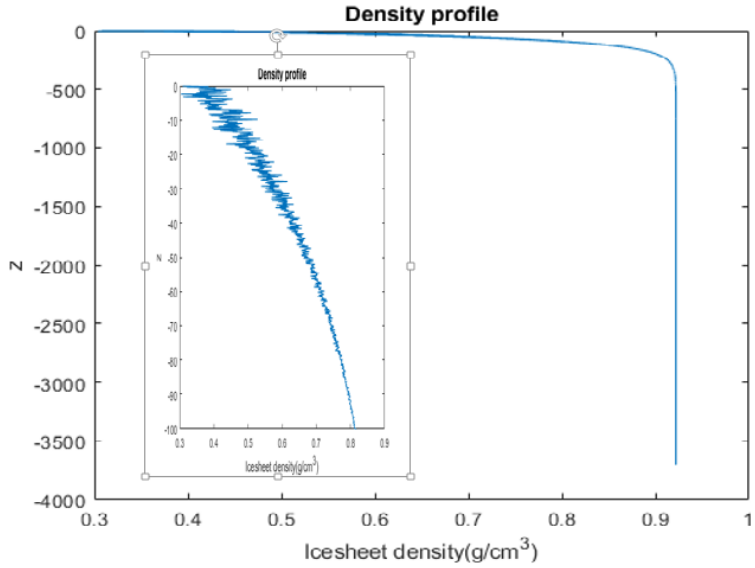

Figure 4. Example ice sheet density profile using $\Delta_1 = 0.04\,\text{g/cc}$, $\ell = 11\,\text{cm}$, $\alpha = 30\,\text{m}$.

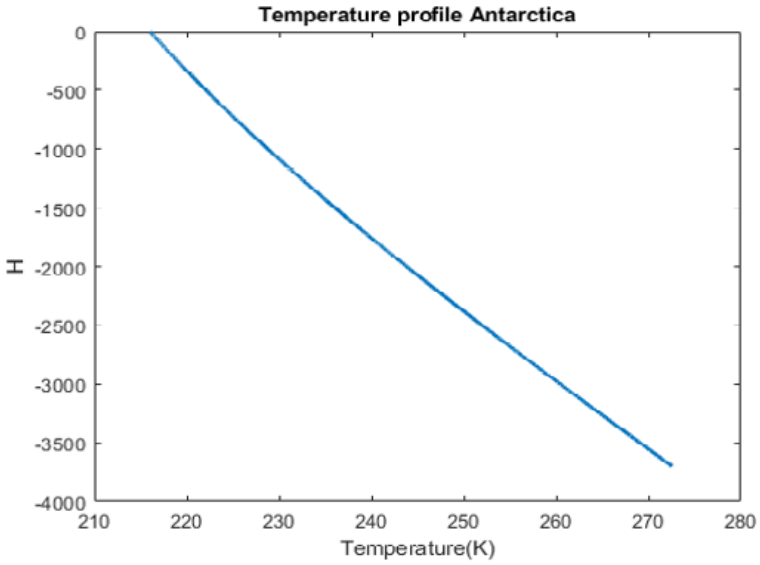

Figure 5. Temperature profile from Robin model with $T_s = 216\,\text{K}$, $M = 0.01\,\text{m/year}$, $G = 0.047\,\text{W/sqm}$ and $H = 3700\,\text{m}$.

realizations of the density random process. The results show that the coherent model and coherent reflectivity model agree well.

The results for 1 density profile realization and a 1000 profile realization average are compared further in Figure 7(a). It is shown that the random profile causes strong fluctuations which is much different from the averaged curve. Figure 7(b) plots the results of Figure 7(a) divided by $(1 - r)$ as would be recommended for canceling cap layer effects in Equation (46). The reflectivity r is simulated here. In the real measurement, it is obtained by radar. The results show that both the single realization and averaged cases recover a smooth lower region brightness temperature that is a function only of the lower region ice temperature and attenuation profiles. To account for the density fluctuations in the passive only approach, a large number of density profiles need to be generated to average out the

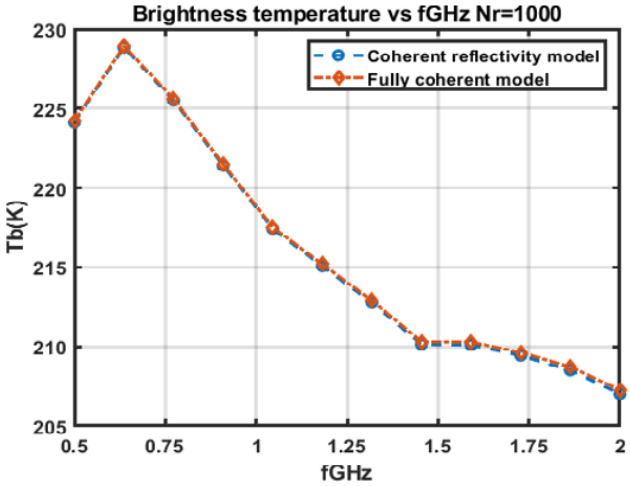

Figure 6. Brightness temperature as a function of frequency, 1000 realization averaging results are shown for coherent model and coherent reflectivity model. The results have shown a good match between the 2 models.

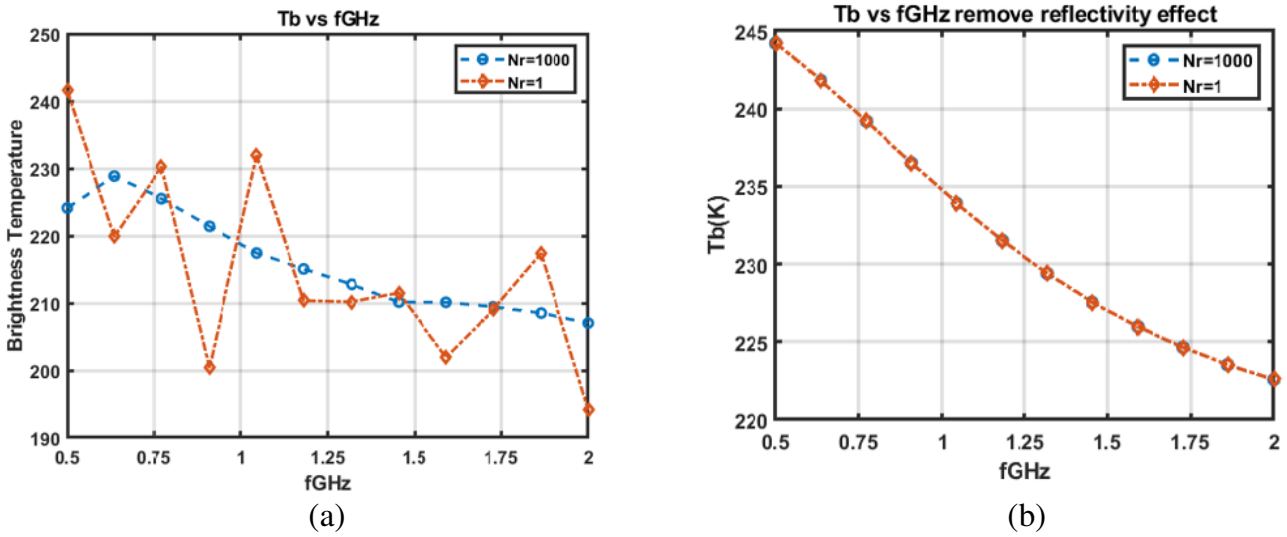

Figure 7. (a) Simulated Brightness temperature as a function of frequency. Results for 1 realization of cap region profiles and 1000 realizations are shown. (b) Simulated brightness temperature with cap region effects compensated. To make the brightness temperature profile stable, we need to use monte carlo averaging to smooth out the fluctuations. With the compensation, the brightness temperature profiles match well with each other for 1 realization and 1000 realizations.

fluctuations as in Figure 7(a). In the combine active and passive method, there is no need to generated profiles since the cap region reflectivity is measured by radar.

Figure 8 again investigates the compensation of cap region effects using a single realization of the brightness temperatures with varying cap layer properties. The results again confirm the applicability of the proposed approach for compensating these effects. In practice for nadiral radiometric measurements, the reflectivity as a function of frequency should be measurable by a nadir pointed radar operating over the same frequency range, indicating the potential for improving temperature profile retrievals using combined active/passive measurements.

Figure 9 shows the case where Equation (47) is not applicable. We use a 1300 m thick ice body with physical temperature profile generated by robin model and $Ts = 250$, $M = 0.32$, $G = 0.1$ are used

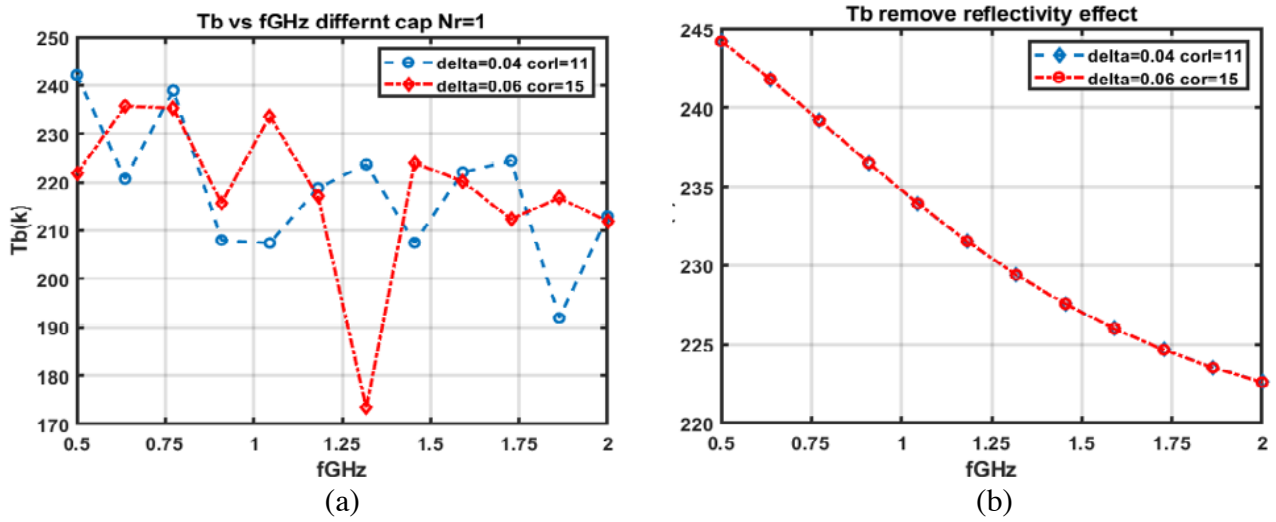

Figure 8. (a) Brightness temperature profile with different cap region properties. (b) Brightness temperature with cap region effect compensation. The results show that for cap regions with different statistical properties, the compensated brightness temperature profiles are the same. In the retrieval process, we do not need a-priori information on the cap region density profiles if we have radar measurements.

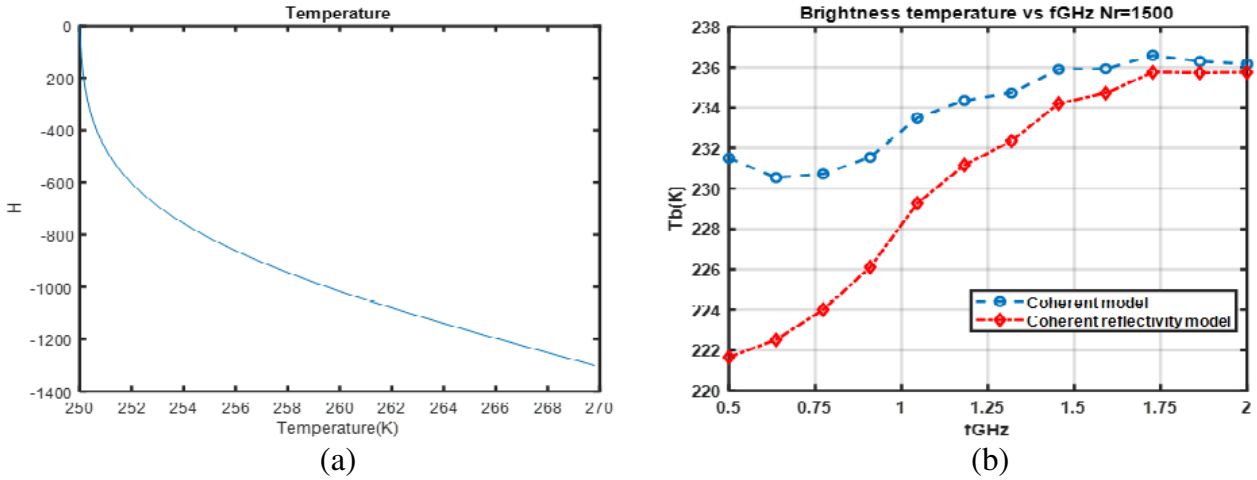

Figure 9. (a) Temperature profile used for the simulation of brightness temperature profile of (b). In this case, the bottom of ice body is water, and the thickness of the ice sheet is not thick enough to be treated as half space. The assumption for the coherent reflectivity model to work is not valid in this case. And as a result, the coherent model predicts a brightness temperature about 10K higher than the results of Equation (51) at the low frequency end due to the reflection from bottom.

as input. We set water below the ice body with $80 + 10i$ as the permittivity. A correlation length of 15 cm is used to generate the top region density fluctuations while the other parameters are the same in the previous case. We only consider the emission from ice body in the coherent model and the coherent reflectivity model as shown in Figure 9(b). In the reflectivity model, we assumed that there is no abrupt change in the profile, which means that the power due to the emission from bottom or reflected from bottom is negligible. Due to the strong reflection at the bottom, the assumption for Equation (47) to work is no longer valid. We may also insert a layer of material into any position in the ice body to break the assumption. Thus the 2 models no longer agree with each other.

7. CONCLUSION

Near surface ice sheet density fluctuations cause reflections that modulate thermal emissions from deeper portions of the ice sheet. In this paper, a coherent reflectivity model for combined active and passive sensing of polar ice sheets was developed. The approximation in the model was shown to characterize the cap region influence in terms of its reflection and transmission coefficients and characterize the emission from ice sheet by it physical temperature profile and absorption profiles. Numerical results show a good agreement with coherent model. The brightness temperature compensated with cap region effects shows smooth curves that are directly related to ice sheet physical temperature and absorption profiles. The model may fail if the condition of "slowly varying profile" is not valid in the large ice body. With the help of radar measurements, the a-priori information of cap region density is not required in the retrieval of ice sheet temperature profiles. The UWBRAD flight path shall extended to the regions without borehole sites. In future work, we shall use the co-located UWBRAD measurement and OIB GPR data to validate this concept.

APPENDIX A. SYMMETRY RELATION OF DYADIC GREEN'S FUNCTION

Let region 0 be homogeneous with permittivity ε and region 1 is inhomogeneous with relative permittivity $\varepsilon_{1r}(\overline{r})$.

First consider a source in region 0.

Let $\overline{a}$ be an arbitrary constant vector located at $\overline{r}_a$. Then the dyadic Green's functions obey the equations

$$\nabla \times \nabla \times \overline{\overline{G}}_{00}(\overline{r}, \overline{r}_a) \cdot \overline{a} - k_0^2 \overline{\overline{G}}_{00}(\overline{r}, \overline{r}_a) \cdot \overline{a} = \overline{a}\delta(\overline{r} - \overline{r}_a) \tag{A1}$$

$$\nabla \times \nabla \times \overline{\overline{G}}_{10}(\overline{r}, \overline{r}_a) \cdot \overline{a} - k_0^2 \varepsilon_{1r}(\overline{r}) \overline{\overline{G}}_{10}(\overline{r}, \overline{r}_a) \cdot \overline{a} = 0 \tag{A2}$$

where $\overline{\overline{G}}_{00}$ denotes a source in region 0 and field point in region 0, and $\overline{\overline{G}}_{10}$ denotes a source in region 0 and field point in region 1.

Boundary conditions on the boundary separating region 0 and region 1 are

$$\widehat{n} \times \overline{\overline{G}}_{00}(\overline{r}, \overline{r}_a) \cdot \overline{a} = \widehat{n} \times \overline{\overline{G}}_{10}(\overline{r}, \overline{r}_a) \cdot \overline{a} \tag{A3}$$

$$\widehat{n} \times \nabla \times \overline{\overline{G}}_{00}(\overline{r}, \overline{r}_a) \cdot \overline{a} = \widehat{n} \times \nabla \times \overline{\overline{G}}_{10}(\overline{r}, \overline{r}_a) \cdot \overline{a} \tag{A4}$$

For a source in region 1, let $\overline{b}$ be an arbitrary constant vector located at $\overline{r}_b$

$$\nabla \times \nabla \times \overline{\overline{G}}_{01}(\overline{r}, \overline{r}_b) \cdot \overline{b} - k_0^2 \overline{\overline{G}}_{01}(\overline{r}, \overline{r}_b) \cdot \overline{b} = 0 \tag{A5}$$

$$\nabla \times \nabla \times \overline{\overline{G}}_{11}(\overline{r}, \overline{r}_b) \cdot \overline{b} - k_0^2 \varepsilon_{1r}(\overline{r}) \overline{\overline{G}}_{11}(\overline{r}, \overline{r}_b) \cdot \overline{b} = \overline{b}\delta(\overline{r} - \overline{r}_b) \tag{A6}$$

The boundary conditions are

$$\widehat{n} \times \overline{\overline{G}}_{01}(\overline{r}, \overline{r}_b) \cdot \overline{b} = \widehat{n} \times \overline{\overline{G}}_{11}(\overline{r}, \overline{r}_b) \cdot \overline{b} \tag{A7}$$

$$\widehat{n} \times \nabla \times \overline{\overline{G}}_{01}(\overline{r}, \overline{r}_b) \cdot \overline{b} = \widehat{n} \times \nabla \times \overline{\overline{G}}_{11}(\overline{r}, \overline{r}_b) \cdot \overline{b} \tag{A8}$$

Applying the vector Green's theorem and integrating over region 0 with $\widehat{n}$ pointing up yields:

$$\int_{region0} dV \left[\left(\overline{\overline{G}}_{01}(\overline{r}, \overline{r}_b) \cdot \overline{b} \right) \cdot \nabla \times \nabla \times \left(\overline{\overline{G}}_{00}(\overline{r}, \overline{r}_a) \cdot \overline{a} \right) - \left(\overline{\overline{G}}_{00}(\overline{r}, \overline{r}_a) \cdot \overline{a} \right) \cdot \nabla \times \nabla \times \left(\overline{\overline{G}}_{01}(\overline{r}, \overline{r}_b) \cdot \overline{b} \right) \right]$$

$$= -\int dS \widehat{n} \cdot \left[\left(\overline{\overline{G}}_{00}(\overline{r}, \overline{r}_a) \cdot \overline{a} \right) \times \nabla \times \left(\overline{\overline{G}}_{01}(\overline{r}, \overline{r}_b) \cdot \overline{b} \right) - \left(\overline{\overline{G}}_{01}(\overline{r}, \overline{r}_b) \cdot \overline{b} \right) \times \nabla \times \left(\overline{\overline{G}}_{00}(\overline{r}, \overline{r}_a) \cdot \overline{a} \right) \right]$$

Then we have

$$\overline{a} \cdot \overline{\overline{G}}_{01}(\overline{r}_a, \overline{r}_b) \cdot \overline{b} = -\int dS \widehat{n} \cdot \left[\left(\overline{\overline{G}}_{00}(\overline{r}, \overline{r}_a) \cdot \overline{a} \right) \times \nabla \times \left(\overline{\overline{G}}_{01}(\overline{r}, \overline{r}_b) \cdot \overline{b} \right) - \left(\overline{\overline{G}}_{01}(\overline{r}, \overline{r}_b) \cdot \overline{b} \right) \times \nabla \times \left(\overline{\overline{G}}_{00}(\overline{r}, \overline{r}_a) \cdot \overline{a} \right) \right] \tag{A9}$$

Next applying vector Green's theorem with a source in region 1 and integrating over region 1 yields:

$$\begin{aligned}
&\int_{region1} dV \Bigg[\left(\overline{\overline{G}}_{11}\left(\overline{r},\overline{r}_b\right)\cdot\overline{b}\right)\cdot\left[k_0^2\varepsilon_{1r}\left(\overline{r}\right)\overline{\overline{G}}_{10}\left(\overline{r},\overline{r}_a\right)\cdot\overline{a}\right] \\
&-\left(\overline{\overline{G}}_{10}\left(\overline{r},\overline{r}_a\right)\cdot\overline{a}\right)\cdot\left[k_0^2\varepsilon_{1r}\left(\overline{r}\right)\overline{\overline{G}}_{11}\left(\overline{r},\overline{r}_b\right)\cdot\overline{b}+\overline{b}\delta\left(\overline{r}-\overline{r}_b\right)\right]\Bigg] \\
&= \int dS\widehat{n}\cdot\left[\left(\overline{\overline{G}}_{10}\left(\overline{r},\overline{r}_a\right)\cdot\overline{a}\right)\times\nabla\times\left(\overline{\overline{G}}_{11}\left(\overline{r},\overline{r}_b\right)\cdot\overline{b}\right)-\left(\overline{\overline{G}}_{11}\left(\overline{r},\overline{r}_b\right)\cdot\overline{b}\right)\times\nabla\times\left(\overline{\overline{G}}_{10}\left(\overline{r},\overline{r}_a\right)\cdot\overline{a}\right)\right]
\end{aligned}$$

Note that

$$\begin{aligned}
&\left(\overline{\overline{G}}_{11}\left(\overline{r},\overline{r}_b\right)\cdot\overline{b}\right)\cdot\left[k_0^2\varepsilon_{1r}\left(\overline{r}\right)\overline{\overline{G}}_{10}\left(\overline{r},\overline{r}_a\right)\cdot\overline{a}\right] \\
&= \left[\overline{\overline{G}}_{10}\left(\overline{r},\overline{r}_a\right)\cdot\overline{a}\right]\cdot\left(k_0^2\varepsilon_{1r}\left(\overline{r}\right)G_{11}\left(\overline{r},\overline{r}_b\right)\cdot\overline{b}\right)-\left(\overline{\overline{G}}_{10}\left(\overline{r}_b,\overline{r}_a\right)\cdot\overline{a}\right)\cdot\overline{b} \\
&= \int dS\widehat{n}\cdot\left[\left(\overline{\overline{G}}_{10}\left(\overline{r},\overline{r}_a\right)\cdot\overline{a}\right)\times\nabla\times\left(\overline{\overline{G}}_{11}\left(\overline{r},\overline{r}_b\right)\cdot\overline{b}\right)-\left(\overline{\overline{G}}_{11}\left(\overline{r},\overline{r}_b\right)\cdot\overline{b}\right)\times\nabla\times\left(\overline{\overline{G}}_{10}\left(\overline{r},\overline{r}_a\right)\cdot\overline{a}\right)\right]
\end{aligned}$$

Applying the boundary conditions, the right hand sides of Equations (1) and (2) are equal and opposite, so that

$$\overline{a}\cdot\overline{\overline{G}}_{01}\left(\overline{r}_a,\overline{r}_b\right)\cdot\overline{b}=\overline{b}\cdot\overline{\overline{G}}_{10}\left(\overline{r}_b,\overline{r}_a\right)\cdot\overline{a} \tag{A10}$$

Since they are scalar, we take transpose amd since $\overline{a}$ and $\overline{b}$ are arbitrary

$$G_{01}\left(\overline{r}_a,\overline{r}_b\right)=G_{10}^t\left(\overline{r}_b,\overline{r}_a\right) \tag{A11}$$

REFERENCES

1. Masson-Delmotte, V., P. Zhai, H. O. Pörtner, D. Roberts, J. Skea, P. R. Shukla, A. Pirani, W. Moufouma-Okia, C. Péan, R. Pidcock, S. Connors, J. B. R. Matthews, Y. Chen, X. Zhou, M. I. Gomis, E. Lonnoy, T. Maycock, M. Tignor, and T. Waterfield, "Global Warming of 1.5°C. An IPCC Special Report on the impacts of global warming of 1.5°C above pre-industrial levels and related global greenhouse gas emission pathways, in the context of strengthening the global response to the threat of climate change, sustainable development, and efforts to eradicate poverty," *IPCC, 2018: Summary for Policymakers, World Meteorological Organization*, Geneva, Switzerland, 2018.
2. Meier, W., G. Hovelsrud, B. van Oort, J. Key, K. Kovacs, C. Michel, C. Hass, M. Granskog, S. Gerland, D. Perovich, A. Makshtas, and J. Reist, "Arctic sea ice in transformation: A review of recent observed changes and impacts on biology and human activity," *Rev. Geophys.*, Vol. 52, 185–217, 2014.
3. Rignot, E., I. Velicogna, M. R. van den Broeke, A. Monaghan, and J. Lenaerts, "Acceleration of the contribution of the Greenland and Antarctic ice sheets to sea level rise," *Geophys. Res. Lett.*, Vol. 38, L05503, 2011.
4. Alley, R. B., P. U. Clark, P. Huybrechts, and I. Joughin, "Ice-sheet and sea-level changes," *Science*, Vol. 310, No. 5747, 456–460, 2005.
5. Jacob, T., J. Wahr, W. T. Pfeffer, and S. Swenson, "Recent contributions of glaciers and ice caps to sea level rise," *Nature*, Vol. 482, No. 7386, 514, 2012.
6. Hock, R., M. de Woul, V. Radić, and M. Dyurgerov, "Mountain glaciers and ice caps around Antarctica make a large sealevel rise contribution," *Geophysical Research Letters*, Vol. 36, L07501, 2012.
7. Zwally, H. J., M. B. Giovinetto, J. Li, H. G. Cornejo, M. A. Beckley, A. C. Brenner, and D. Yi, "Mass changes of the Greenland and Antarctic ice sheets and shelves and contributions to sea-level rise: 1992–2002," *Journal of Glaciology*, Vol. 51, No. 175, 509–527, 2005.
8. Matsuoka, K., R. C. Hindmarsh, G. Moholdt, M. J. Bentley, H. D. Pritchard, J. Brown, and T. Hattermann, "Antarctic ice rises and rumples: Their properties and significance for ice-sheet dynamics and evolution," *Earth-Science Reviews*, Vol. 150, 724–745, 2015.

9. Gagliardini, O., G. Durand, T. Zwinger, R. C. A. Hindmarsh, and E. Le Meur, "Coupling of iceshelf melting and buttressing is a key process in ice-sheets dynamics," *Geophysical Research Letters*, Vol. 37, L14501, 2010.
10. Matelli, E. and C. Schoof, "Thermally-activated sliding in ice sheet flow," *American Geophysical Union, Fall Meeting 2018*, 2018.
11. Mantelli, E. and C. Schoof, "Ice sheet dynamics with temperature-dependent sliding," *Geophysical Research Abstracts*, Vol. 21, EGU2019-10993-5, 2019.
12. Hill, B., et al., "Using radio-wave attenuation to constrain ice temperature in regions of fast flow," *American Geophysical Union, Fall Meeting 2018*, 2018.
13. Winebrenner, D. P., S. Tyler, and J. Selker, "Diagnosis of glacier and ice bed dynamics by means of Raman distributed temperature sensing and melt-probe deployment," *American Geophysical Union, Fall Meeting 2018*, 2018.
14. Forster, R. R., J. E. Box, M. R. van den Broeke, C. Miège, E. W. Burgess, J. H. van Angelen, et al., "Extensive liquid meltwater storage in firn within the Greenland ice sheet," *Nat. Geosci.*, Vol. 7, 95–98, 2014.
15. Miller, O., D. K. Solomon, C. Miège, L. S. Koenig, R. R. Forster, L. N. Montgomery, N. Schmerr, S. R. M. Ligtenberg, A. Legchenko, and L. Brucker, "Hydraulic conductivity of a Firn Aquifer in Southeast Greenland," *Front. Earth Sci.*, Vol. 5, No. 38, doi: 10.3389/feart.2017.00038, 2017.
16. Andrews, M. J., et al., "The ultrawideband software-defined microwave radiometer: Instrument description and initial campaign results," *IEEE Trans. Geosci. Remote. Sens.*, Vol. 56, No. 10, 5923–5935, Oct. 2018.
17. Johnson, J., K. Jezek, M. Andrews, M. Durand, Y. Duan, C. Yardim, A. Bringer, G. Macelloni, M. Brogioni, S. Tan, and L. Tsang, "Measurement of ice sheet internal temperature profiles with ultrawidebandmicrowave radiometry," *American Geophysical Union, Fall Meeting 2018*, 2018.
18. Yardim, C., J. T. Johnson, K. C. Jezek, M. Andrews, M. Durand, Y. Duan, S. Tan, L. Tsang, M. Brogioni, G. Macelloni, and A. Bringer, "Greenland ice sheet subsurface temperature estimation using ultra-wideband microwave radiometry," *IEEE Trans. Geosc. Rem. Sens.*, 2019.
19. Tsang, L. and J. A. Kong, *Scattering of Electromagnetic Waves: Theories and Applications*, Ch. 5, Vol. 1, 203–217, Wiley, Hoboken, NJ, USA, 2000.
20. Rytov, S. M., *Theory of Electromagnetic Radiation and Fluctuations*, Publishing House, Academy of Science, USSR, 1953.
21. Tan, S., et al., "Physical models of layered polar firn brightness temperatures from 0.5 to 2 GHz," *IEEE J. Sel. Topics Appl. Earth Observ. Remote Sens.*, Vol. 8, No. 7, 3681–3691, Jul. 2015.
22. Tan, S., L. Tsang, H. Xu, J. T. Johnson, K. C. Jezek, C. Yardim, M. Durand, and Y. Duan, "A partially coherent approach for modelong polar ice sheet 0.5–2 GHz thermal emission," *IEEE Trans. Geosc. Rem. Sens.*, 2019.
23. Van der Veen, J., *Fundamentals of Glacier Dynamics*, A. A. Balkema, 462, Rotterdam, The Netherlands, 1999.
24. Mätzler, C. and A. Wiesmann, "Extension of the microwave emission model of layered snowpacks to coarse-grained snow," *Remote Sens. Environ.*, Vol. 70, 317–325, 1999.
25. Mätzler, C., "Microwave permittivity of dry snow," *IEEE Trans. Geosci. Remote. Sens.*, Vol. 34, No. 2, 573–581, Mar. 1996.
26. Tiuri, M. E., A. H. Sihvola, E. G. Nyfors, and M. T. Hallikainen, "The complex dielectric constant of snow at microwave frequencies," *IEEE J. Oceanic Eng.*, Vol. 9, No. 5, 377–382, Dec. 1984.